Radiology: Artificial Intelligence

ORIGINAL RESEARCH

Deep Learning–based Approach for Brainstem and Ventricular MR Planimetry: Application in Patients with Progressive Supranuclear Palsy

Salvatore Nigro, PhD • Marco Filardi, PhD • Benedetta Tafuri, PhD • Martina Nicolardi, MD • Roberto De Blasi, MD • Alessia Giugno, MD • Valentina Gnoni, MD, PhD • Giammarco Milella, MD • Daniele Urso, MD • Stefano Zoccolella, MD • Giancarlo Logroscino, MD, PhD • for the Frontotemporal Lobar Degeneration Neuroimaging Initiative, for the 4-Repeat Tau Neuroimaging Initiative[1] • for the Alzheimer's Disease Neuroimaging Initiative[2]

From the Center for Neurodegenerative Diseases and the Aging Brain, University of Bari Aldo Moro, Pia Fondazione Cardinale G. Panico, 73039 Tricase, Italy (S.N., M.F., B.T., A.G., V.G., D.U., G.L.); Department of Translational Biomedicine and Neuroscience (DiBraiN), University of Bari Aldo Moro, Bari, Italy (M.F., B.T., G.M., G.L.); Department of Radiology, Pia Fondazione Cardinale G. Panico, Tricase, Italy (M.N., R.D.B.); Department of Neurosciences, Institute of Psychiatry, Psychology and Neuroscience, King's College London, London, England (D.U.); and Operative Unit of Neurology, San Paolo Hospital, ASL Bari, Bari, Italy (S.Z.). Received May 5, 2023; revision requested July 18; revision received February 1, 2024; accepted March 6. **Address correspondence to** S.N. (email: *salvatoreangelo.nigro@gmail.com*).

[1]Data used in preparation of this article were obtained from the Frontotemporal Lobar Degeneration Neuroimaging Initiative (FTLDNI) database *(http://4rtni-fildni.ini.usc.edu/)*. The investigators at NIFD/FTLDNI contributed to the design and implementation of FTLDNI and/or provided data but did not participate in analysis or writing of this report (unless otherwise listed).

[2]Data used in preparation of this article were obtained from the Alzheimer's Disease Neuroimaging Initiative (ADNI) database (adni.loni.usc.edu). As such, the investigators within the ADNI contributed to the design and implementation of ADNI and/or provided data but did not participate in analysis or writing of this report. A complete listing of ADNI investigators can be found at: *http://adni.loni.usc.edu/wp-content/uploads/how_to_apply/ADNI_Acknowledgement_List.pdf*.

Supported by the Regione Puglia and CNR for Tecnopolo per la Medicina di Precisione, DGR number 2117 of November 21, 2018 (CUPB84I18000540002), and the Research Center of Excellence for Neurodegenerative Diseases and Brain Aging (CIREMIC), University of Bari, Aldo Moro.

Conflicts of interest are listed at the end of this article.

See also the commentary by Mohajer in this issue.

Radiology: Artificial Intelligence 2024; 6(3):e230151 • https://doi.org/10.1148/ryai.230151 • Content codes: AI MR NR

Purpose: To develop a fast and fully automated deep learning (DL)–based method for the MRI planimetric segmentation and measurement of the brainstem and ventricular structures most affected in patients with progressive supranuclear palsy (PSP).

Materials and Methods: In this retrospective study, T1-weighted MR images in healthy controls (n = 84) were used to train DL models for segmenting the midbrain, pons, middle cerebellar peduncle (MCP), superior cerebellar peduncle (SCP), third ventricle, and frontal horns (FHs). Internal, external, and clinical test datasets (n = 305) were used to assess segmentation model reliability. DL masks from test datasets were used to automatically extract midbrain and pons areas and the width of MCP, SCP, third ventricle, and FHs. Automated measurements were compared with those manually performed by an expert radiologist. Finally, these measures were combined to calculate the midbrain to pons area ratio, MR parkinsonism index (MRPI), and MRPI 2.0, which were used to differentiate patients with PSP (n = 71) from those with Parkinson disease (PD) (n = 129).

Results: Dice coefficients above 0.85 were found for all brain regions when comparing manual and DL-based segmentations. A strong correlation was observed between automated and manual measurements (Spearman $\rho > 0.80$, $P < .001$). DL-based measurements showed excellent performance in differentiating patients with PSP from those with PD, with an area under the receiver operating characteristic curve above 0.92.

Conclusion: The automated approach successfully segmented and measured the brainstem and ventricular structures. DL-based models may represent a useful approach to support the diagnosis of PSP and potentially other conditions associated with brainstem and ventricular alterations.

Supplemental material is available for this article.

Quantitative MRI analysis plays an important role in characterizing brain changes associated with aging processes and neurodegenerative diseases (1–3). Brain morphometric features based on MRI segmentation have been proven able to provide unique information for differentiating patients with parkinsonian syndromes (4,5). In particular, brainstem and ventricular planimetric measurements have been proposed as reliable and informative imaging biomarkers to support the diagnosis of progressive supranuclear palsy (PSP) (4,6–9). Indeed, several studies have consistently shown that the degree of atrophy of these regions accurately differentiates patients with PSP from patients with other atypical parkinsonian disorders and Parkinson disease (PD), and combined planimetric measures of the brainstem, namely the midbrain to pons area ratio (MP) and the MR parkinsonism index (MRPI), are considered level 3 diagnostic biomarkers for PSP (6,10–13). More recently, a new version of the MRPI (ie, MRPI 2.0) that includes combined planimetric measures of brainstem and ventricular regions has been developed and showed

Abbreviations

AUC = area under the receiver operating characteristic curve, DL = deep learning, FHs = frontal horns, MCP = middle cerebellar peduncle, MP = midbrain to pons area ratio, MRPI = magnetic resonance parkinsonism index, PSP = progressive supranuclear palsy, SCP = superior cerebellar peduncle

Summary

The deep learning–based method developed using T1-weighted MR images provided fast and accurate planimetric segmentations and measurements of the brainstem and ventricular structures most affected in patients with progressive supranuclear palsy.

Key Points

- A deep learning–based method provided robust brainstem and ventricular segmentation on T1-weighted images compared to manual-based segmentation (mean Dice coefficients > 0.85).
- The automated approach took less than 2 minutes per case to segment and measure specific brainstem and ventricular structures.
- The deep learning–based approach proved to be a valuable tool for assisting radiologists in the fast and accurate assessment of planimetric measurements of brainstem and ventricular regions, which are primarily affected in patients with progressive supranuclear palsy.

Keywords

MR Imaging, Brain/Brain Stem, Segmentation, Quantification, Diagnosis, Convolutional Neural Network

higher accuracy than MRPI in differentiating patients with PSP parkinsonism from patients with PD (14).

Currently, manual segmentation is considered the reference standard for planimetric and volumetric measurements of brain structures at MRI. However, this approach is time- and resource-demanding and prone to inter- and intrarater variability, especially for small brain regions, thus limiting the usability of the above-mentioned neuroimaging biomarkers in routine clinical practice (15). To overcome these issues, several studies have developed semi- or fully automated segmentation methods, adopting threshold- and landmark-based approaches (13,16,17), as well as atlas-based segmentation strategies (18,19). This decade, deep learning (DL) techniques have also been employed for the rapid and accurate segmentation of brain regions (20–22). DL models learn to capture relevant features from raw images through a sequence of contracting and expanding paths of convolutions (encoder and decoder components) and generate as final output the desired segmentation masks (23,24). However, to the best of our knowledge, DL-based segmentation has never been applied to the planimetric segmentation and measurement of brainstem and ventricular regions.

In the current study, we developed and validated an automated approach for the planimetric segmentation and measurement of brainstem and ventricular structures using DL-based models on volumetric T1-weighted MR images. First, DL-based segmentation models were trained to automatically delineate the midbrain and pons, middle and superior cerebellar peduncles, and the third and lateral ventricles. Second, the accuracy of each DL-based segmentation model was assessed on internal, external, and clinical test datasets. Third, DL-based segmentations were used to automatically quantify the area of midbrain and pons, the width of the middle cerebellar peduncle (MCP) and superior cerebellar peduncle (SCP), and the width of the third ventricle and frontal horns (FHs). Finally, these planimetric measurements were combined to calculate the MP, MRPI, and MRPI 2.0 and differentiate patients with PSP from those with PD.

Materials and Methods

Dataset Description

In this retrospective study, a total of 389 T1-weighted images were used for training and testing of each DL model (Table 1). First, we randomly selected 120 controls (age range, 40–80 years) from the Parkinson's Progression Markers Initiative dataset *(https://www.ppmi-info.org/access-data-specimens/download-data)*. A 70:30 ratio was used to split the sample into the training (n = 84; mean age, 60.41 years ± 12.73 [SD]) and internal test (n = 36; mean age, 58.51 years ± 9.86) datasets. One individual was excluded from the internal test dataset due to signal intensity artifacts in the data. Next, 35 controls (mean age, 61.51 years ± 7.38) from the Frontotemporal Lobar Degeneration Neuroimaging Initiative *(https://4rtni-ftldni.ini.usc.edu/)* and 35 (mean age, 65.37 years ± 4.53) from the Alzheimer's Disease Neuroimaging Initiative *(https://adni.loni.usc.edu/)* were used as external test sets. Finally, MR images in 71 patients with PSP–Richardson syndrome, (58 [mean age, 70.57 years ± 7.16] from the 4-Repeat Tauopathy Neuroimaging Initiative *[http://4rtni-ftldni.ini.usc.edu]* and 13 [mean age, 70.46 years ± 3.07] from the Center for Neurodegenerative Diseases and the Aging Brain of the University of Bari at Pia Fondazione Cardinale G. Panico) and 129 age- and sex-matched patients with PD (98 [mean age, 68.45 years ± 5.51 years] from the Parkinson's Progression Markers Initiative dataset and 31 [mean age, 69.88 years ± 5.34 years] from the Center for Neurodegenerative Diseases and the Aging Brain) were used as clinical test dataset. T1-weighted images were acquired with 1.5-T and 3-T MRI scanners from different vendors and with a wide variety of high-resolution sequences (Table S1). All individuals provided informed consent, and the protocol was approved by the institutional review board at all sites.

Preprocessing

MR images were first processed with Automatic Registration Toolbox software (ART; Nitric *https://www.nitrc.org/projects/art*) to automatically reorient images and define the midsagittal section and the anterior and the poster commissures (25,26); the images were then resampled into a 256 × 256 × 512-mm^3 volume. Next, the intensity range of each two-dimensional section used for manual segmentation and as input for the DL-based models was individually transformed to a 0–1 range using min-max normalization.

Manual Segmentations

Manual segmentations of brainstem and ventricular regions were performed on preprocessed T1-weighted images by a radiologist (R.D.B., with more than 30 years of experience as

Table 1: Demographic Data of Individuals Included in Training, Internal, External, and Clinical Test Datasets

	Training Dataset	Internal Test Dataset	External Test Dataset		Clinical Test Dataset			
Variable	PPMI HC (*n* = 84)	PPMI HC (*n* = 35)	FTLDNI HC (*n* = 35)	ADNI HC (*n* = 35)	PPMI PD (*n* = 98)	4RTNI PSP (*n* = 58)	CMND PD (*n* = 31)	CMND PSP (*n* = 13)
Male/female ratio	50:34	20:15	12:23	14:21	46:52	24:34	20:11	9:4
Age (y)*	60.41 ± 12.73	58.51 ± 9.86	61.81 ± 7.38	65.37 ± 4.53	68.45 ± 5.51	70.57 ± 7.16	69.88 ± 5.34	70.46 ± 3.07
MRI manufacturer	Philips GE Siemens	Philips GE Siemens	Siemens	Philips GE Siemens	Philips GE Siemens	Siemens	Philips	Philips

Note.—Unless otherwise specified, data are numbers. ADNI = Alzheimer's Disease Neuroimaging Initiative, CMND = Center for Neurodegenerative Diseases and the Aging Brain, 4RTNI = 4-Repeat Tauopathy Neuroimaging Initiative, FTLDNI = Frontotemporal Lobar Degeneration Neuroimaging Initiative, HC = healthy controls, PD = Parkinson disease, PPMI = Parkinson's Progression Markers Initiative, PSP = progressive supranuclear palsy.
* Values are means ± SDs.

a neuroradiologist), who was blinded to the patients' diagnoses. Manual segmentation of the midbrain and pons was performed as described in previous studies (10,11). In particular, the midbrain tegmentum and a line passing through the superior pontine notch and the inferior edge of the quadrigeminal plate were used to define the upper and bottom borders of the midbrain, respectively. A second line, parallel to the first line passing through the inferior pontine notch, was drawn to define the margins of the pons. The MCP masks were drawn in 12 consecutive sections around the midsagittal plane using the regions of interest previously described in Nigro et al (13). These sections were automatically chosen to expose the MCP between the pons and the cerebellum. For manual segmentation of the SCP, MR images were first automatically reformatted in the anteroposterior direction to identify the first view on which inferior colliculi and SCPs were separated (13). Subsequently, manual segmentation of the SCP was performed in three consecutive sections. To expose the third ventricle and the FHs of the lateral ventricles, T1-weighted images were automatically reformatted in axial view using the anterior commissure–posterior commissure plane (14). Next, the third ventricle was segmented on the axial section generated at the level of both the anterior and posterior commissures, and the FHs were delineated on 10 consecutive axial sections. All manual segmentations were performed using an in-house–developed tool.

ResNet50 Architecture for Automated Segmentation

MR images exposing brainstem and ventricular regions of interest and corresponding manual segmentations were used as input to construct DL models (Fig 1). Specifically, a DL-based segmentation model was developed for each target structure by using a network based on encoder-decoder architecture, that is, ResNet-50–U-Net (27,28). The encoder ResNet-50 extracted features from the original image, and the decoder U-Net completed the fusion of information based on these features, thereby completing the pixel-by-pixel prediction of input image. In more detail, ResNet-50 is a 50-layer convolutional neural network that uses skip connections to propagate information over layers, allowing for increased depth of the network and higher performance levels compared with other models (27). The ResNet-50 was pretrained on the ImageNet 2012 classification dataset *(https://www.image-net.org/)*, which comprises 1000 classes and 1.28 million training images. The pretrained weights were obtained from a public repository *(https://github.com/fchollet/deep-learning-models/releases/download/v0.2/resnet50_weights_tf_dim_ordering_tf_kernels.h5)*. The training of each DL model was performed in five epochs using the Adam optimizer with an initial learning rate of 0.01. Moreover, data augmentation was used to increase the size of the training dataset to enhance the performance of DL models. Specifically, data augmentation was achieved by rotating ($-30° < \text{angle } \theta < 30°$) and translating images by −20% to 20% on the x- and y-axis independently. All models were implemented in a Keras framework *(https://github.com/keras-team)*, with Python version 3.6.9 and TensorFlow version 2.4.1 on an NVIDIA Quadro RTX 4000 (8 GB) graphics processing unit. Codes are available at *https://github.com/divamgupta/image-segmentation-keras*.

Automated Planimetric Measurements Using DL-based Segmentations

The pipeline for the automated DL-based segmentation and measurement of brainstem and ventricular structures is shown in Figure 2. Using the DL outputs, the midbrain and pons areas were calculated by counting the number of pixels belonging to each mask. Next, the MCP width was quantified by extracting the contour of each DL-based binary mask and then calculating the distances between the most caudal point of the upper profile and the most rostral point of the inferior profile (13). For the SCP width, the symmetry axis was automatically defined for the left and right peduncle masks, and the width of each structure was calculated as the largest distance between the medial and lateral borders of the mask (13). This procedure was applied on the three consecutive sections, and the average SCP width was

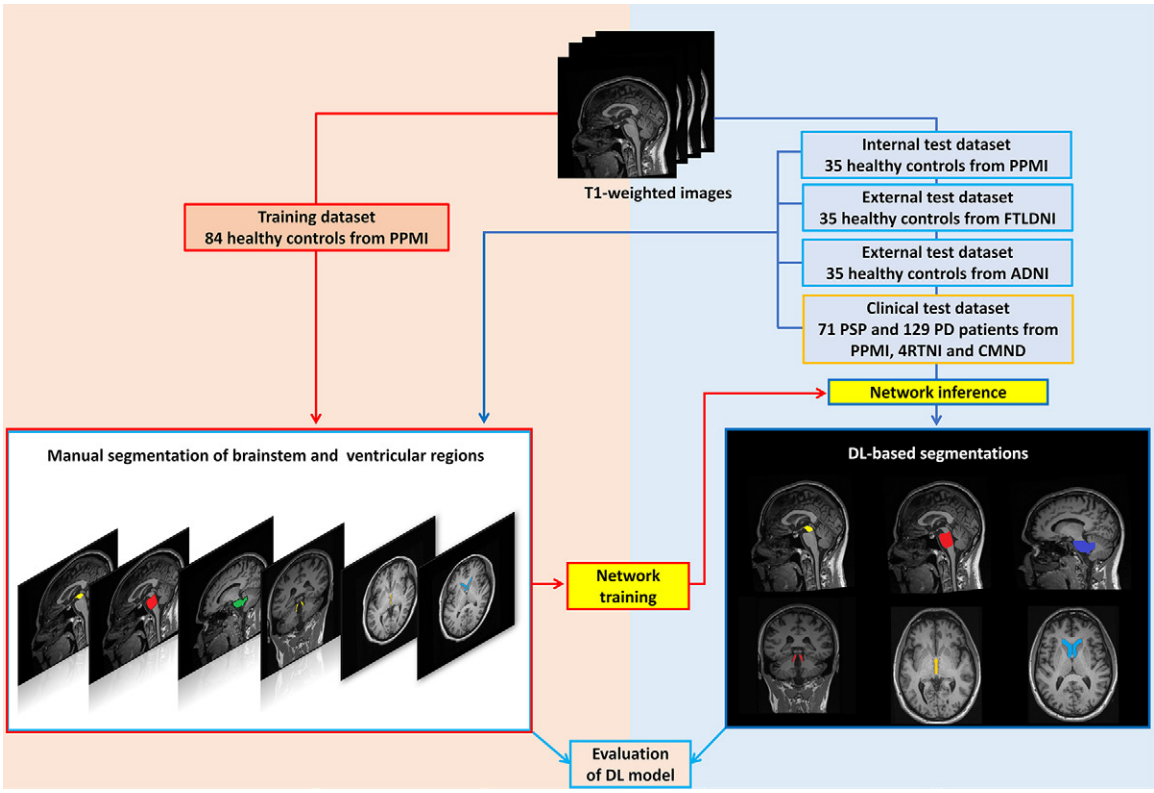

Figure 1: Data processing for deep learning (DL) model training and testing. Manual segmentations of the brainstem and ventricular regions were performed using preprocessed T1-weighted images from the training dataset (red arrows). The neural networks were then trained using manual segmentations (left panel). The trained models were applied to internal, external, and clinical test images (blue arrows) to output the masks of midbrain, pons, middle cerebellar peduncles, superior cerebellar peduncles, third ventricles, and frontal horns (right panel). Finally, the performance of the DL-based models was evaluated by comparing the pixelwise agreement between the predicted segmentation and its corresponding manual ground truth. ADNI = Alzheimer's Disease Neuroimaging Initiative, CMND = Center for Neurodegenerative Diseases and the Aging Brain, 4RTNI = 4-Repeat Tauopathy Neuroimaging Initiative, FTLDNI = Frontotemporal Lobar Degeneration Neuroimaging Initiative, PD = Parkinson disease, PPMI = Parkinson's Progression Markers Initiative, PSP = progressive supranuclear palsy.

calculated. The third ventricle width was defined as the maximum distance between the lateral borders of its mask. For each axial section showing the FHs of the lateral ventricles, the largest width was considered (17) as the maximum distance between left to right FHs. Finally, MP, MRPI, and MRPI 2.0 were calculated as previously described (10,11,14).

Statistical Analysis

To explore accuracy of the DL results, automated segmentations were compared to manual tracing by calculating Dice coefficients in the internal, external, and clinical test datasets. In particular, the Dice score was calculated using the following formula: $(2\times TP)/[(TP+FP)+(TP+FN)]$, where TP, FP, and FN indicated the number of true-positive, false-positive, and false-negative pixels, respectively. A Dice score of 1 reflects a perfect spatial correspondence between the automated and manual masks, whereas a score of 0 indicates no agreement. As an additional measure of the DL models' efficacy, automated planimetric measurements conducted on DL-based masks were compared to those manually performed by an experienced radiologist as described in previous studies (10,11). The Mann-Whitney *U* test was used to assess differences between automated and manual measurements for each brain region. The agreement between automated and manual measures was assessed through Spearman rank correlation coefficient analysis and concordance correlation coefficients. Moreover, Spearman correlation analysis was used to assess the relationship between brainstem and ventricular planimetric features. Receiver operating characteristic curve analysis was used to assess the diagnostic performance (area under the receiver operating characteristic curve [AUC], sensitivity, and specificity) of planimetric measurements in differentiating patients with PSP from those with PD. The Youden index (ie, sensitivity + specificity −1) was used to identify the optimal cutoff values. Finally, the AUCs of DL-based and manual measurements of the MP, MRPI, and MRPI 2.0 were compared using the nonparametric methods developed by DeLong et al (29). Statistical analyses were performed using MATLAB R2021a version 9.10.0 (MathWorks). *P* values less than .05 were considered statistically significant.

Results

Comparison of Manual and Automated Segmentations in Internal, External, and Clinical Datasets

Figure 3 shows box plots of the Dice overlap for each brain structure in the internal, external, and clinical test sets. The mean Dice scores comparing automated to manual segmentations were higher than 0.90 for the midbrain, pons, MCP,

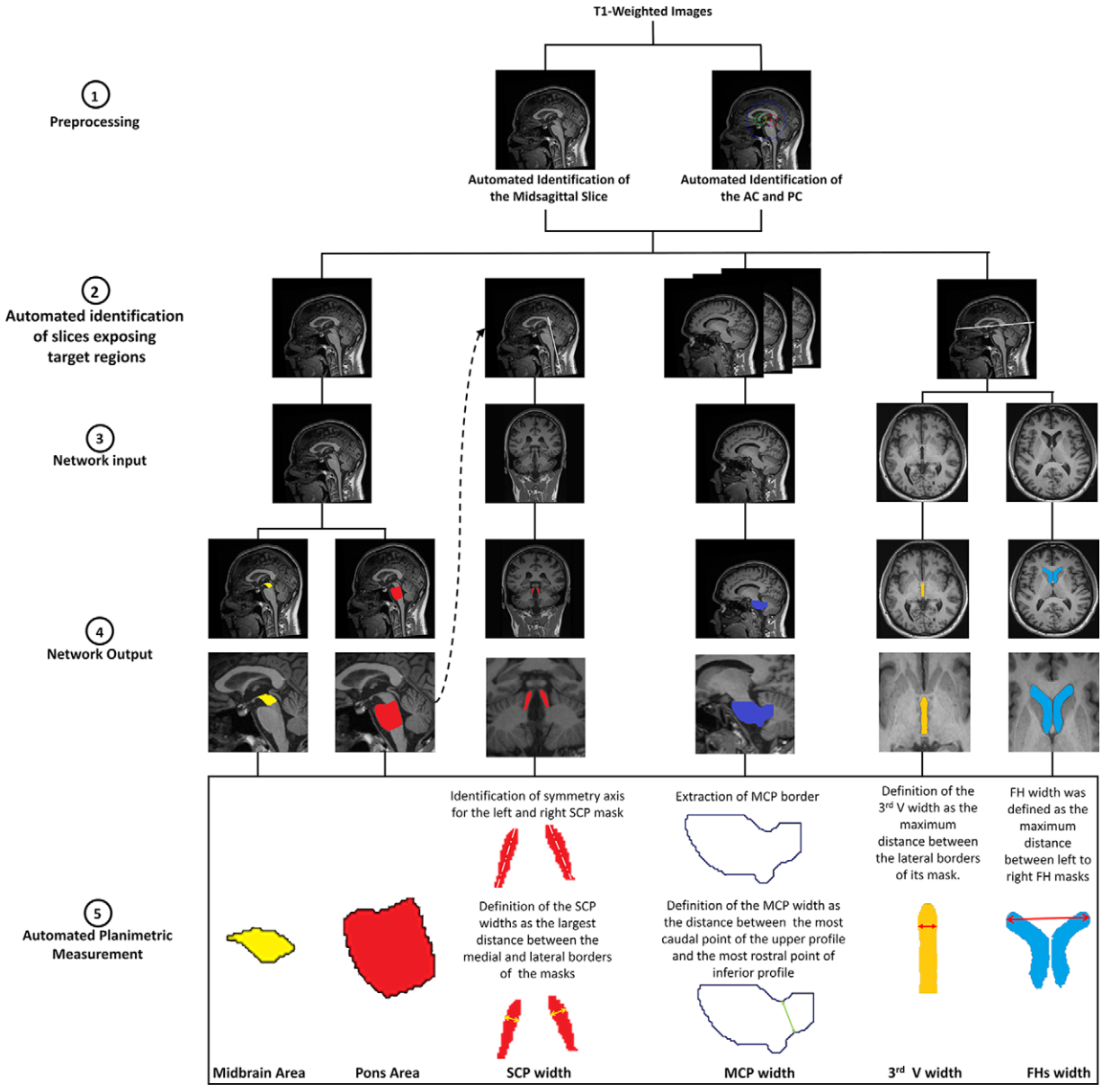

Figure 2: Pipeline for the automated planimetric deep learning–based segmentation and measurement of the brainstem and ventricular structures. AC = anterior commissure, FH = frontal horn, MCP = middle cerebellar peduncle, PC = posterior commissure, SCP = superior cerebellar peduncle, 3rd V = third ventricle.

third ventricle, and FHs in each dataset and were 0.87, 0.89, and 0.88 for the SCP on the internal, external, and clinical test sets, respectively. A graphic representation of the DL-based segmentation outputs is shown in Figure 4.

Comparison between Manual and Automated Measurements in Internal, External, and Clinical Datasets

No evidence of differences was found between automated and manual measurements for the internal and external test datasets (Table 2). A significant correlation emerged, for both datasets, between automated and manual measurements for all brain regions (Spearman correlation coefficient ranging between 0.80 and 0.96) (Fig 5). A correlation coefficient of 0.90 or higher was found between automated and manual values for the midbrain, pons, third ventricle, and FHs, while a correlation coefficient equal to 0.89 and 0.80 was found for the MCP and SCP, respectively. The strong agreement between automated and manual measurement was also shown by the concordance correlation coefficients, with values above 0.80 for all brain structures (Fig 5). No evidence of differences was found between automated and manual measurements for patients with PD and PSP (Table 3). Finally, a strong correlation was observed between automated and manual measurements for all brain structures, with Spearman correlation coefficients ranging between 0.84 and 0.99 (Figs S1 and S2).

Evaluation of DL-based and Manual Planimetric Measurements in Patients with PD and PSP

A significant difference in automated measurements of the single brain regions was found between patients with PSP and

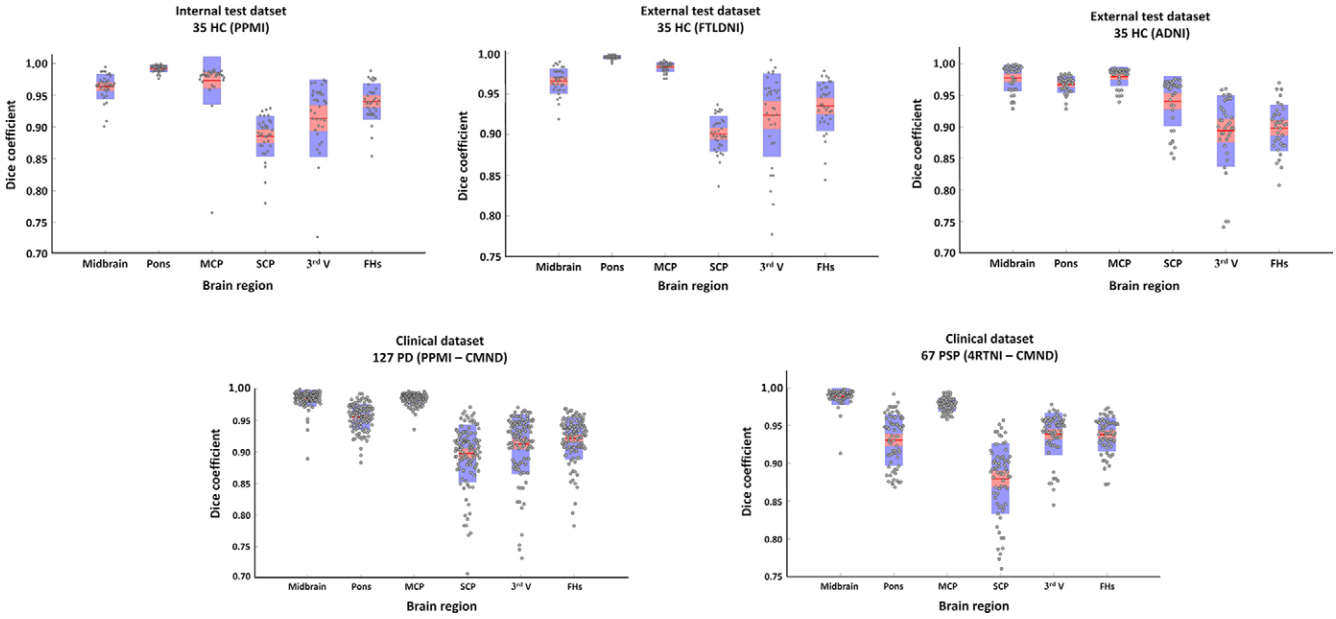

Figure 3: Comparison of automatic and manual segmentations, using Dice similarity coefficients, in the internal, external, and clinical test datasets. ADNI = Alzheimer's Disease Neuroimaging Initiative, CMND = Center for Neurodegenerative Diseases and the Aging Brain, 4RTNI = 4-Repeat Tauopathy Neuroimaging Initiative, FHs = frontal horns, FTLDNI = Frontotemporal Lobar Degeneration Neuroimaging Initiative, HC = healthy controls, MCP = middle cerebellar peduncle, PD = Parkinson disease, PPMI = Parkinson's Progression Markers Initiative, PSP = progressive supranuclear palsy, SCP = superior cerebellar peduncle, 3rd V = third ventricle.

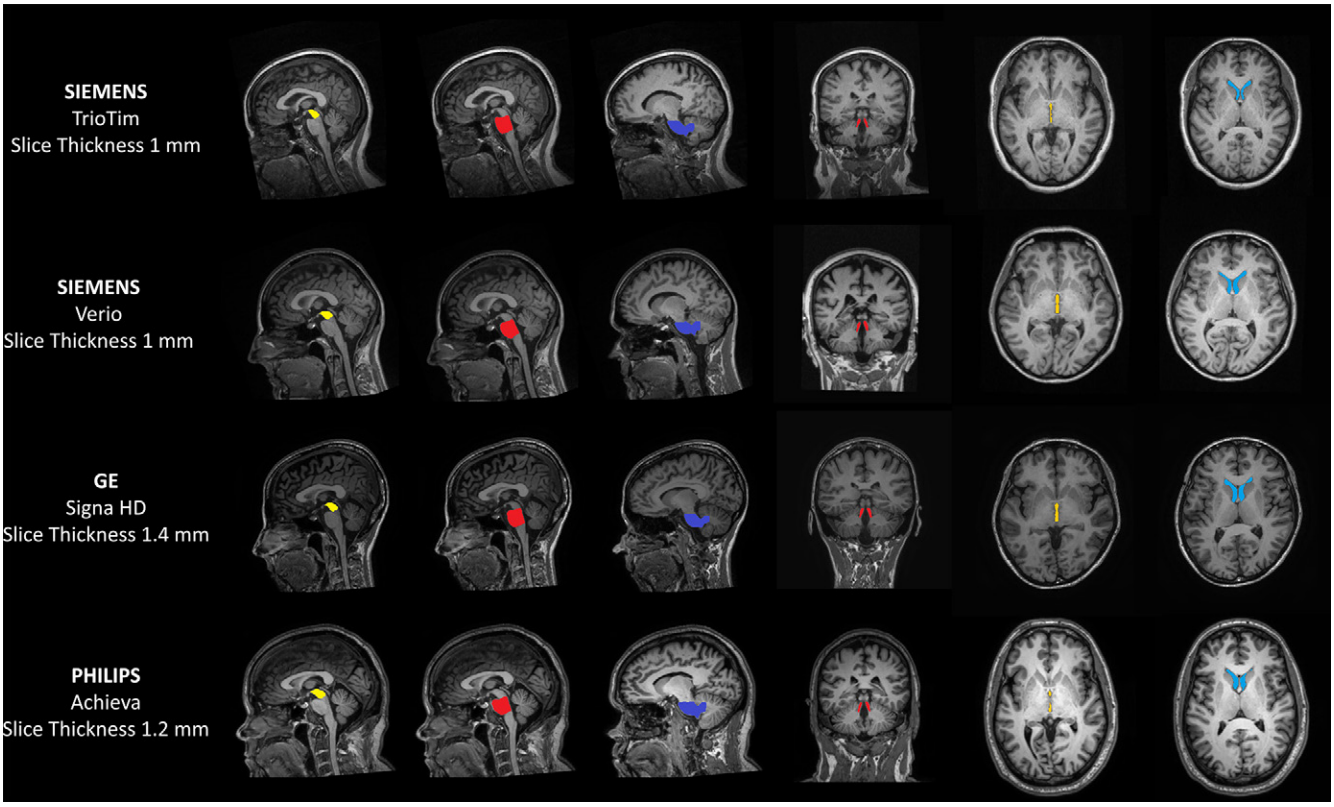

Figure 4: Examples of automated deep learning–based segmentations performed on T1-weighted images acquired with different scanner manufacturers and MRI protocols.

patients with PD (Table 3, Fig 6). Correlation analyses also revealed significant relationships among brainstem and ventricular planimetric features (Fig S3). Concerning combined planimetric indices, automated MP values were significantly lower in patients with PSP (median = 0.15, range = 0.10–0.26) than in patients with PD (median = 0.24, range = 0.19–0.30). Automated MRPI and MRPI 2.0 values were significantly higher in patients with PSP (MRPI: median = 17.38, range = 7.69–

Table 2: Manual and Automatic Measurements of Brainstem and Ventricular Regions, MP, MRPI, and MRPI 2.0 in Test Datasets

	Internal Test Dataset (PPMI)		External Test Dataset (FTLDNI)		External Test Dataset (ADNI)	
Parameter	Automated Measurements	Manual Measurements	Automated Measurements	Manual Measurements	Automated Measurements	Manual Measurements
Midbrain (mm^2)	141.69 ± 18.24	141.31 ± 18.21	137.09 ± 20.22	135.34 ± 21.61	136.91 ± 13.02	142.86 ± 14.64
Pons (mm^2)	535.09 ± 47.61	527.40 ± 43.36	532.97 ± 61.19	520.23 ± 63.70	537.20 ± 54.90	538.91 ± 55.31
MCP (mm)	9.21 ± 1.23	8.90 ± 0.94	9.75 ± 0.72	9.31 ± 0.76	9.39 ± 1.07	9.21 ± 1.00
SCP (mm)	3.52 ± 0.46	3.55 ± 0.37	3.66 ± 0.40	3.66 ± 0.38	3.76 ± 0.30	3.67 ± 0.40
Third ventricle (mm)	4.31 ± 1.42	4.48 ± 1.38	4.29 ± 1.74	4.5 ± 1.4	4.41 ± 1.93	4.77 ± 1.89
FHs (mm)	33.60 ± 3.34	34.33 ± 2.91	33.57 ± 3.45	34.45 ± 3.95	33.38 ± 4.55	32.80 ± 4.66
MP	0.27 ± 0.03	0.27 ± 0.03	0.26 ± 0.03	0.26 ± 0.03	0.26 ± 0.03	0.27 ± 0.03
MRPI	10.06 ± 1.80	9.52 ± 1.47	10.55 ± 1.67	9.95 ± 1.39	9.89 ± 1.68	9.63 ± 1.81
MRPI 2.0	1.28 ± 0.41	1.24 ± 0.43	1.36 ± 0.60	1.34 ± 0.52	1.31 ± 0.58	1.42 ± 0.61

Note.—Values are means ± SDs. Each dataset consists of 35 healthy controls. No evidence of statistically significant differences was found in each dataset between automated and manual measurements. ADNI = Alzheimer's Disease Neuroimaging Initiative, FHs= frontal horns, FTLDNI = Frontotemporal Lobar Degeneration Neuroimaging Initiative, MCP = middle cerebellar peduncle, MP = midbrain to pons area ratio, MRPI = MR parkinsonism index, PPMI = Parkinson's Progression Markers Initiative, SCP = superior cerebellar peduncle.

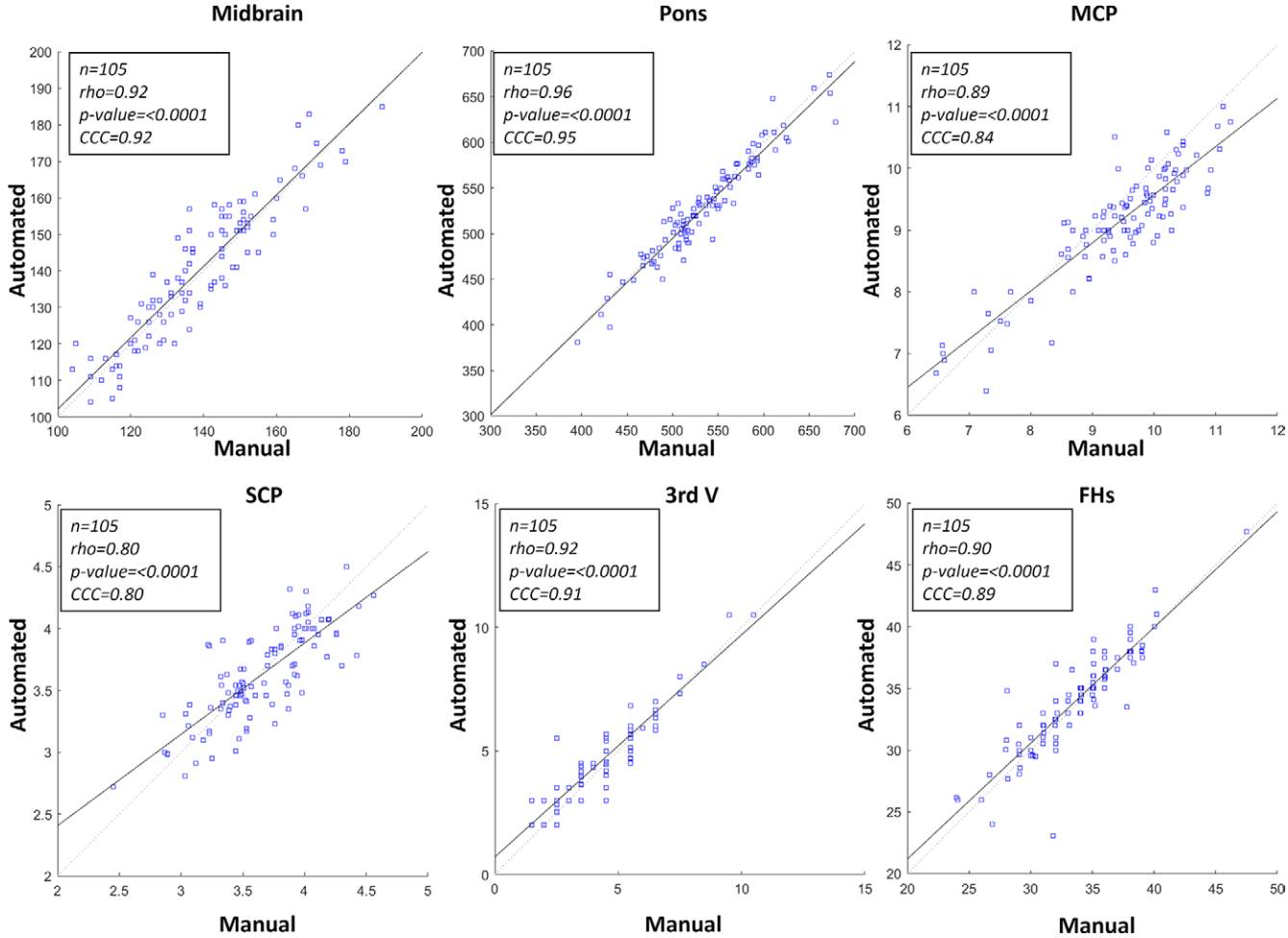

Figure 5: Correlations between manual and automated planimetric measurements in internal and external test datasets. CCC = concordance correlation coefficient, FHs = frontal horns, MCP = middle cerebellar peduncle, rho = Spearman correlation coefficient, SCP = superior cerebellar peduncle, 3rd V = third ventricle.

Table 3: Automated and Manual Measurements of Brainstem and Ventricular Regions, MP, MRPI, and MRPI 2.0 in Patients with PSP and Patients with PD

	Automated Measurements		Manual Measurements	
Parameter	Mean ± SD	Range	Mean ± SD	Range
Patients with PD (n = 127)				
Midbrain (mm^2)	128.35 ± 16.56	84–172	133.61 ±17.16	85–181
Pons (mm^2)	533.72 ± 52.51	414–662	546.61 ± 54.44	421–680
MCP (mm)	9.30 ± 0.87	6.7–11.42	9.27 ± 0.93	6.20–11.03
SCP (mm)	3.72 ± 0.47	2.41–5.04	3.66 ± 0.46	2.51–5.11
3rd V (mm)	5.80 ± 1.98	1.50–11.50	6.22 ± 2.00	2.00–11.50
FHs (mm)	36.45 ± 4.29	27.02–51.09	35.51 ± 4.48	23.00–51.01
MP	0.24 ± 0.03	0.19–0.30	0.24 ± 0.03	0.18–0.35
MRPI	10.64 ± 1.85	6.81–17.69	10.59 ± 1.85	6.84–17.01
MRPI 2.0	1.70 ± 0.62	0.35–3.31	1.86 ± 0.67	0.55–4.10
Patients with PSP (n = 67)				
Midbrain (mm^2)	73.31 ± 17.44	41–132	76.91 ± 16.53	42–127
Pons (mm^2)	463.61 ± 59.91	344–623	470.46 ± 58.81	356–627
MCP (mm)	8.39 ± 1.05	5.67–10.40	8.31 ± 0.98	5.30–11.00
SCP (mm)	3.11 ± 0.45	2.10–4.24	2.94 ± 0.50	2.00–4.35
3rd V (mm)	8.27 ± 2.36	1.50–14.50	8.91 ± 2.56	1.00–15.00
FHs (mm)	39.10 ± 4.86	31.02–51.00	38.05 ± 4.83	29.50–49.09
MP	0.16 ± 0.03	0.10–0.26	0.16 ± 0.03	0.10–0.24
MRPI	18.01 ± 5.51	7.69–38.71	18.39 ± 5.44	7.83–35.92
MRPI 2.0	3.85 ± 1.65	0.78–9.16	4.30 ± 1.89	0.48–9.15

Note.—FHs = frontal horns, MCP = middle cerebellar peduncle, MP = midbrain to pons area ratio, MRPI = MR parkinsonism index, PD = Parkinson disease, PSP = progressive supranuclear palsy, SCP = superior cerebellar peduncle, 3rd V = third ventricle.

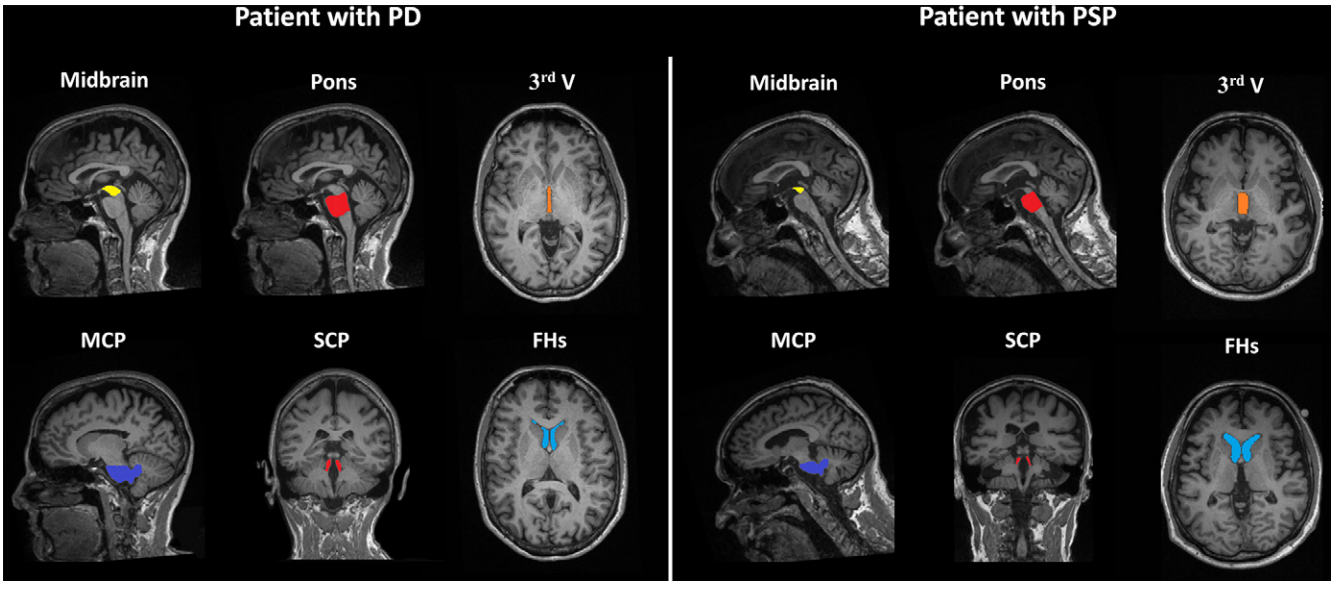

Figure 6: Automated planimetric segmentation of midbrain, pons, MCP, SCP, third ventricle, and frontal horns in a 72-year-old male patient with PD and a 75-year-old male patient with PSP. FHs = frontal horns, MCP = middle cerebellar peduncle, PD = Parkinson disease, PSP = progressive supranuclear palsy, SCP = superior cerebellar peduncle, 3rd V = third ventricle.

Table 4: Diagnostic Performance of Automated and Manual MP, MRPI, and MRPI 2.0 in Differentiating Patients with PSP from Those with PD

Parameter	Automated	Manual	*P* Value
MP			
Cutoff value	<0.20	<0.20	
Sensitivity (%)	90 (60/67)	88 (59/67)	
Specificity (%)	96 (123/127)	95 (121/127)	
AUC	0.97 (0.94, 0.99)	0.97 (0.95, 0.99)	>.99
MRPI			
Cutoff value	>12.94	>13.00	
Sensitivity (%)	90 (60/67)	88 (59/67)	
Specificity (%)	95 (121/127)	94 (119/127)	
AUC	0.95 (0.92, 0.99)	0.95 (0.91, 0.99)	.87
MPRI 2.0			
Cutoff value	>2.29	>2.41	
Sensitivity (%)	90 (60/67)	87 (58/67)	
Specificity (%)	84 (107/127)	86 (109/127)	
AUC	0.92 (0.88, 0.97)	0.92 (0.88, 0.96)	.97

Note.—AUCs are presented with 95% CIs in parentheses. Sensitivity and specificity are presented as percentages, with numerators and denominators in parentheses. AUC = area under the receiver operating characteristic curve, MP = midbrain to pons area ratio, MRPI = MR parkinsonism index, PD = Parkinson disease, PSP = progressive supranuclear palsy.

38.71; MRPI 2.0: median = 3.49, range = 0.78–9.16) than in those with PD (MRPI: median = 10.66, range = 6.81–17.69; MRPI 2.0: median = 1.61, range = 0.35–3.31) (Table 3). Similar results were obtained when considering manual measurements (Table 3). Automated planimetric measurements were successfully completed in 97% of cases (194 of 200 total patients); in six cases, the automated approach failed to identify the midsagittal section, leading to incorrect DL-based segmentations and measurements.

Performance of Automated and Manual Measurement in Differentiating Patients with PSP from those with PD

Sensitivity, specificity, and AUC for the automated MP, MRPI, and MRPI 2.0 are reported in Table 4. In the receiver operating characteristic curve analyses, all MRI indices showed an AUC higher than 0.92 in distinguishing patients with PD from patients with PSP. An automated MP value of 0.20 showed 90% sensitivity (60 of 67) and 97% specificity (123 of 127) in differentiating patients with PSP from patients with PD. An MRPI value of 12.94 showed 90% sensitivity (60 of 67) and 95% specificity (121 of 127) in differentiating patients with PSP from those with PD. Finally, an automated MRPI 2.0 value of 2.29 showed 90% sensitivity (60 of 67) and 84% specificity (107 of 127) in differentiating the two groups. Similar classification performance was observed using manual measurements. No evidence of differences was observed in AUC values for MP, MRPI, and MRPI 2.0 between automated and manual approaches (Table 4).

Discussion

In this study, we developed a fully automated, DL-based method using T1-weighted MR images that enables fast and accurate segmentation and measurement of brainstem and ventricular areas most affected in patients with PSP. We observed a high spatial overlap between manual and DL-based masks of the midbrain, pons, MCP and SCP, and third ventricle and FHs (mean Dice coefficients > 0.85). For each region, high agreement was also observed between manual and automated planimetric measurements obtained using DL outputs (Spearman correlation coefficients > 0.80). Moreover, automated measurements showed high accuracy in differentiating patients with PSP from those with PD (AUCs > 0.92 for MP, MRPI, and MRPI 2.0).

Over the past few decades, several automated approaches have been proposed for defining brainstem and ventricular regions (13,16,17,19,30–32). Volumetric approaches have been developed to automatically assess brainstem and ventricular atrophy in several pathologic conditions, using atlas- and DL-based methods (16,18,19,30–33). In particular, DL-based methods implementing multidimensional gated recurrent units and three-dimensional convolutional neural networks with the U-Net architecture have been used this decade to perform accurate volumetry of the ventricles and brainstem, respectively (30,32). Although volumetric approaches could potentially be used to extract planimetric information from specific sections, it is important to note that this solution is not feasible for the particular brain regions

investigated in our study due to the lack of a publicly available atlas for three-dimensional segmentation of the MCP on T1-weighted MR images. Moreover, calculating planimetric measures, such as the width of the SCP, requires the identification of specific planes to expose structures of interest, making the use of three-dimensional masks challenging and time-consuming.

Concerning planimetric assessments, automated methods aimed to identify regions of interest using information about the morphology and position of predefined brain structures (13,17). A thresholding-based approach was also used to separate each region from the background by comparing the intensity values of each pixel to a predefined threshold. Moreover, different threshold values were proposed for 1.5-T and 3-T scanners (13). However, errors in the identification of automated anatomic landmarks may arise due to the changes in brain region dimensions associated with interindividual variability and pathologic conditions (6,17). Additionally, in the case of image noise and/or other imaging artifacts, using only first-order features, such as image intensity, may not be sufficient for an accurate brain MRI segmentation (34). To mitigate these problems, existing methods introduced a preprocessing step to register MR images to a standard space and then correct for fluctuation in intensity using the FreeSurfer software package *(https://surfer.nmr.mgh.harvard.edu/)* (35). Nonetheless, a percentage of failures ranging from 4% to 7.5% was commonly reported for the automated segmentation of brainstem and ventricular regions using the latter approaches (6,13,17). It is noteworthy that the addition of a preprocessing stage substantially increases calculation times (approximately equal to 15 minutes) and the amount of computational resources, making these approaches difficult to use in clinical routines where the time available and the number of resources are often limited.

The present study extended prior efforts by proposing a new approach that uses DL models to perform a faster, more reliable, and generalizable segmentation of brainstem and ventricular structures. Compared to previous approaches, our method requires solely an intensity-normalization preprocessing step to identify regions of interest without the need for a priori anatomic information. This leads to a substantial reduction in segmentation and measurement times (total computational time approximately equal to 2 minutes), while ensuring a negligible rate of failures (ie, 3%). Notably, our method outperforms the manual approach in terms of time, with the latter requiring approximately 10 minutes per individual for brainstem and ventricular segmentation and measurement.

In terms of segmentation accuracy, an average Dice value higher than 0.85 between manual and automated segmentations was observed for each brain region in controls, patients with PD, and patients with PSP. This suggests that the trained model can successfully perform accurate segmentations in pathologic conditions, such as PSP–Richardson syndrome, that are characterized by marked anatomic alterations in the brainstem and ventricular structures. Specifically, we found a mean Dice coefficient above 0.90 for the midbrain, pons, and ventricular regions, in line with previous studies (16,19,30–33). A lower mean Dice coefficient (0.87) was found for the SCP, possibly due to its smaller size compared to the other regions under consideration. Similarly, concerning planimetric assessment, manual and automated measurements showed a strong agreement ($\rho > 0.80$) in controls, patients with PD, and patients with PSP–Richardson syndrome. Finally, PSP imaging biomarkers (ie, MP, MRPI, and MRPI 2.0) computed using the DL-based method exhibited an AUC higher than 0.92 in distinguishing between patient groups, consistent with previous classification studies using automated approaches (4,6,13,17). Notably, the cutoffs identified in this study are consistent with those previously reported in patients with PSP (6,13,14), thereby providing further evidence of the robustness of these MRI indices for PSP diagnosis.

Some limitations of the present study must be acknowledged. First, manual delineation of the brainstem and ventricular regions was performed by a single rater, although with more than 30 years of experience in the field of neuroradiology. Second, PD and PSP cases were not pathologically confirmed. Moreover, we considered only patients with PSP–Richardson syndrome, and further studies are needed to investigate the robustness and usefulness of our approach in other clinical subtypes, such as PSP parkinsonism, and/or considering patients at early disease stages. Third, during the models' training phase, we did not adopt early stopping criteria and cross-validation. Although this can lead to overfitting issues, the optimal segmentation performance displayed by DL-based models in the independent external test datasets indicates their generalizability on new MR images. Fourth, a min-max intensity normalization method was used to transform the image intensity range of MR images used as input to DL-based models. While this approach is commonly used to transform the intensity histogram to a 0–1 range without affecting the image itself, it may be influenced by outliers in the raw intensity values. Finally, although our results showed clear-cut differences between patients with PD and patients with PSP in MP, MRPI, and MRPI 2.0, it is important to highlight that these indices are computed based on brainstem and ventricular morphologic features that are significantly correlated. A high degree of collinearity may increase the risk of observing statistically significant results by chance and make the determination of the individual contribution of each brain region to the indices challenging.

In conclusion, we showed that planimetric quantification of brainstem and ventricular substructures on T1-weighted MR images can be automatically and rapidly performed using a DL-based segmentation approach. Our DL-based segmentation method overcomes the limitations of the previous automated methods and has important implications in the field of neuroradiology. The possibility of using our solution to obtain a rapid and reliable computation of MRI biomarkers for PSP has the potential to lead to more widespread use of brainstem and ventricular planimetry in clinical practice. Moreover, DL masks might be used to extract information on tissue changes that go beyond the classical morphometric properties, such as radiomics features, thus providing complementary information that could potentially improve the differential diagnosis between parkinsonian disorders.

Acknowledgments: Data used in the preparation of this manuscript were obtained from the Parkinson's Progression Markers Initiative (PPMI) database *(https://www.ppmi-info.org/access-data-specimens/download-data)*, the 4-Repeat Neuroimaging Initiative (4RTNI) database, the Frontotemporal Lobar Degeneration Neuroimaging Initiative (FTLDNI) *(http://4rtni-ftldni.ini.usc.edu)* and from the Alzheimer's Disease Neuroimaging Initiative (ADNI, *https://adni.loni.usc.edu/*). For up-to-date information on the PPMI study, visit *www.ppmi-info.org*. PPMI— a public-private partnership—is funded by the Michael J. Fox Foundation for Parkinson's Research and funding partners, including 4D Pharma, AbbVie Inc., AcureX Therapeutics, Allergan, Amathus Therapeutics, Aligning Science Across Parkinson's (ASAP), Avid Radiopharmaceuticals, Bial Biotech, Biogen, BioLegend, BlueRock Therapeutics, Bristol Myers Squibb, Calico Life Sciences LLC, Celgene Corporation, DaCapo Brainscience, Denali Therapeutics, The Edmond J. Safra Foundation, Eli Lilly and Company, Gain Therapeutics, GE HealthCare, GlaxoSmithKline, Golub Capital, Handl Therapeutics, Insitro, Janssen Pharmaceuticals, Lundbeck, Merck & Co., Inc., Meso Scale Diagnostics, LLC, Neurocrine Biosciences, Pfizer Inc., Piramal Imaging, Prevail Therapeutics, F. Hoffmann-La Roche Ltd and its affiliated company Genentech Inc., Sanofi Genzyme, Servier, Takeda Pharmaceutical Company, Teva Neuroscience, Inc., UCB, Vanqua Bio, Verily Life Sciences, Voyager Therapeutics, Inc., Yumanity Therapeutics, Inc. 4RTNI was launched in early 2011 and is funded through the National Institute of Aging and The Tau Research Consortium. The primary goal of 4RTNI is to identify neuroimaging and biomarker indicators for disease progression in the 4-repeat tauopathy neurodegenerative diseases, progressive supranuclear palsy (PSP) and corticobasal degeneration (CBD). FTLDNI is also funded through the National Institute of Aging and started in 2010. The primary goals of FTLDNI are to identify neuroimaging modalities and methods of analysis for tracking frontotemporal lobar degeneration (FTLD) and to assess the value of imaging versus other biomarkers in diagnostic roles. The principal investigator of 4RTNI is Adam Boxer, MD, PhD, at the University of California, San Francisco. The data is the result of collaborative efforts at four sites in North America. For more information on 4RTNI, please visit *http://memory.ucsf.edu/research/studies/4rtni*. The principal investigator of NIFD is Howard Rosen, MD at the University of California, San Francisco. The data is the result of collaborative efforts at three sites in North America. For up-to-date information on participation and protocol, please visit *http://memory.ucsf.edu/research/studies/nifd*. Data used in the preparation of this article were obtained from the Alzheimer's Disease Neuroimaging Initiative (ADNI) database (adni.loni.usc.edu). The ADNI was launched in 2003 as a public-private partnership, led by principal investigator Michael W. Weiner, MD. The primary goal of ADNI has been to test whether serial MRI, PET, other biological markers, and clinical and neuropsychological assessment can be combined to measure the progression of mild cognitive impairment and early Alzheimer's disease. For up-to-date information, see *www.adni-info.org*. Data collection and sharing for this project was funded by the Alzheimer's Disease Neuroimaging Initiative (ADNI) (National Institutes of Health grant U01 AG024904) and DOD ADNI (Department of Defense award no. W81XWH-12-2-0012). ADNI is funded by the National Institute on Aging, the National Institute of Biomedical Imaging and Bioengineering, and through generous contributions from the following: AbbVie, Alzheimer's Association; Alzheimer's Drug Discovery Foundation; Araclon Biotech; BioClinica, Inc.; Biogen; Bristol-Myers Squibb Company; CereSpir, Inc.; Cogstate; Eisai Inc.; Elan Pharmaceuticals, Inc.; Eli Lilly and Company; EuroImmun; F. Hoffmann-La Roche Ltd and its affiliated company Genentech, Inc.; Fujirebio; GE Healthcare; IXICO Ltd.; Janssen Alzheimer Immunotherapy Research & Development, LLC.; Johnson & Johnson Pharmaceutical Research & Development LLC.; Lumosity; Lundbeck; Merck & Co., Inc.; Meso Scale Diagnostics, LLC.; NeuroRx Research; Neurotrack Technologies; Novartis Pharmaceuticals Corporation; Pfizer Inc.; Piramal Imaging; Servier; Takeda Pharmaceutical Company; and Transition Therapeutics. The Canadian Institutes of Health Research is providing funds to support ADNI clinical sites in Canada. Private sector contributions are facilitated by the Foundation for the National Institutes of Health *(www.fnih.org)*. The grantee organization is the Northern California Institute for Research and Education, and the study is coordinated by the Alzheimer's Therapeutic Research Institute at the University of Southern California. ADNI data are disseminated by the Laboratory for Neuro Imaging at the University of Southern California. Anonymized for review.

Author contributions: Guarantors of integrity of entire study, **S.N., B.T., M.N., R.D.B., A.G., G.L.**; study concepts/study design or data acquisition or data analysis/interpretation, all authors; manuscript drafting or manuscript revision for important intellectual content, all authors; approval of final version of submitted manuscript, all authors; agrees to ensure any questions related to the work are appropriately resolved, all authors; literature research, **S.N., B.T., M.N., R.D.B., A.G., V.G., G.M., S.Z., G.L.**; clinical studies, **M.N., A.G., V.G.**; experimental studies, **B.T., M.N., A.G., V.G.**; statistical analysis, **S.N., B.T., M.N., A.G., S.Z.**; and manuscript editing, **S.N., M.F., M.N., R.D.B., A.G., V.G., G.M., D.U., S.Z., G.L.**

Data sharing: Data analyzed during the study were provided by a third party. Requests for data should be directed to the providers indicated in the Acknowledgments.

Disclosures of conflicts of interest: S.N. Funding from Regione Puglia and CNR for Tecnopolo per la Medicina di Precisione, DGR number 2117 of November 21, 2018 (CUPB84I18000540002), the Research Center of Excellence for Neurodegenerative Diseases and Brain Aging (CIREMIC), University of Bari, Aldo Moro. **M.F.** Funding from Regione Puglia and CNR for Tecnopolo per la Medicina di Precisione, DGR number 2117 of November 21, 2018 (CUPB84I18000540002), the Research Center of Excellence for Neurodegenerative Diseases and Brain Aging (CIREMIC), University of Bari, Aldo Moro. **B.T.** No relevant relationships. **M.N.** No relevant relationships. **R.D.B.** No relevant relationships. **A.G.** No relevant relationships. **V.G.** No relevant relationships. **G.M.** disclosed no relevant relationships. **D.U.** No relevant relationships. **S.Z.** No relevant relationships. **G.L.** Funding from Regione Puglia and CNR for Tecnopolo per la Medicina di Precisione, DGR number 2117 of November 21, 2018 (CUPB84I18000540002), the Research Center of Excellence for Neurodegenerative Diseases and Brain Aging (CIREMIC), University of Bari, Aldo Moro.

References

1. Seiler A, Nöth U, Hok P, et al. Multiparametric quantitative MRI in neurological diseases. Front Neurol 2021;12:640239.
2. McEvoy LK, Brewer JB. Quantitative structural MRI for early detection of Alzheimer's disease. Expert Rev Neurother 2010;10(11):1675–1688.
3. Koikkalainen J, Rhodius-Meester H, Tolonen A, et al. Differential diagnosis of neurodegenerative diseases using structural MRI data. Neuroimage Clin 2016;11:435–449.
4. Illán-Gala I, Nigro S, VandeVrede L, et al. Diagnostic accuracy of magnetic resonance imaging measures of brain atrophy across the spectrum of progressive supranuclear palsy and corticobasal degeneration. JAMA Netw Open 2022;5(4):e229588. [Published correction appears in JAMA Netw Open 2022;5(5):e2217977.]
5. Scotton WJ, Bocchetta M, Todd E, et al. A data-driven model of brain volume changes in progressive supranuclear palsy. Brain Commun 2022;4(3):fcac098.
6. Nigro S, Antonini A, Vaillancourt DE, et al. Automated MRI classification in progressive supranuclear palsy: a large international cohort study. Mov Disord 2020;35(6):976–983.
7. Cooperrider J, Bluett B, Jones SE. Methods and utility of quantitative brainstem measurements in progressive supranuclear palsy versus Parkinson's disease in a routine clinical setting. Clin Park Relat Disord 2020;3:100033.
8. Nigro S, Morelli M, Arabia G, et al. Magnetic Resonance Parkinsonism Index and midbrain to pons ratio: Which index better distinguishes Progressive Supranuclear Palsy patients with a low degree of diagnostic certainty from patients with Parkinson Disease? Parkinsonism Relat Disord 2017;41:31–36.
9. Sjöström H, Granberg T, Hashim F, Westman E, Svenningsson P. Automated brainstem volumetry can aid in the diagnostics of parkinsonian disorders. Parkinsonism Relat Disord 2020;79:18–25.
10. Quattrone A, Nicoletti G, Messina D, et al. MR imaging index for differentiation of progressive supranuclear palsy from Parkinson disease and the Parkinson variant of multiple system atrophy. Radiology 2008;246(1):214–221.
11. Oba H, Yagishita A, Terada H, et al. New and reliable MRI diagnosis for progressive supranuclear palsy. Neurology 2005;64(12):2050–2055.
12. Whitwell JL, Höglinger GU, Antonini A, et al. Radiological biomarkers for diagnosis in PSP: Where are we and where do we need to be? Mov Disord 2017;32(7):955–971.
13. Nigro S, Arabia G, Antonini A, et al. Magnetic Resonance Parkinsonism Index: diagnostic accuracy of a fully automated algorithm in comparison with the manual measurement in a large Italian multicentre study in patients with progressive supranuclear palsy. Eur Radiol 2017;27(6):2665–2675.
14. Quattrone A, Morelli M, Nigro S, et al. A new MR imaging index for differentiation of progressive supranuclear palsy-parkinsonism from Parkinson's disease. Parkinsonism Relat Disord 2018;54:3–8.
15. Obuchowicz R, Oszust M, Piorkowski A. Interobserver variability in quality assessment of magnetic resonance images. BMC Med Imaging 2020;20(1):109.
16. Nigro S, Cerasa A, Zito G, et al. Fully automated segmentation of the pons and midbrain using human T1 MR brain images. PLoS One 2014;9(1):e85618.
17. Quattrone A, Bianco MG, Antonini A, et al. Development and validation of automated Magnetic Resonance Parkinsonism Index 2.0 to distinguish progressive supranuclear palsy-parkinsonism from Parkinson's disease. Mov Disord 2022;37(6):1272–1281.
18. Iglesias JE, Sabuncu MR. Multi-atlas segmentation of biomedical images: A survey. Med Image Anal 2015;24(1):205–219.
19. Iglesias JE, Van Leemput K, Bhatt P, et al. Bayesian segmentation of brainstem structures in MRI. Neuroimage 2015;113:184–195.
20. Dünnwald M, Ernst P, Düzel E, Tönnies K, Betts MJ, Oeltze-Jafra S. Fully automated deep learning-based localization and segmentation of the locus coeruleus in aging and Parkinson's disease using neuromelanin-sensitive MRI. Int J CARS 2021;16(12):2129–2135.

21. Beliveau V, Nørgaard M, Birkl C, Seppi K, Scherfler C. Automated segmentation of deep brain nuclei using convolutional neural networks and susceptibility weighted imaging. Hum Brain Mapp 2021;42(15): 4809–4822.
22. Wachinger C, Reuter M, Klein T. DeepNAT: Deep convolutional neural network for segmenting neuroanatomy. Neuroimage 2018;170:434–445.
23. Akkus Z, Galimzianova A, Hoogi A, Rubin DL, Erickson BJ. Deep learning for brain MRI segmentation: state of the art and future directions. J Digit Imaging 2017;30(4):449–459.
24. Hinton G. Deep learning-a technology with the potential to transform health care. JAMA 2018;320(11):1101–1102.
25. Ardekani BA, Bachman AH. Model-based automatic detection of the anterior and posterior commissures on MRI scans. Neuroimage 2009;46(3):677–682.
26. Ardekani BA, Kershaw J, Braun M, Kanno I. Automatic detection of the mid-sagittal plane in 3-D brain images. IEEE Trans Med Imaging 1997;16(6):947–952.
27. He K, Zhang X, Ren S, Sun J. Deep residual learning for image recognition. 2016 IEEE Conference on Computer Vision and Pattern Recognition (CVPR). IEEE, 2016; 770–778.
28. Ronneberger O, Fischer P, Brox T. U-Net: convolutional networks for biomedical image segmentation. In: Navab N, Hornegger J, Wells WM, Frangi AF, eds. Medical Image Computing and Computer-Assisted Intervention – MICCAI 2015. MICCAI 2015. Lecture Notes in Computer Science, vol 9351. Springer, 2015; 234–241.
29. DeLong ER, DeLong DM, Clarke-Pearson DL. Comparing the areas under two or more correlated receiver operating characteristic curves: a nonparametric approach. Biometrics 1988;44(3):837–845.
30. Shao M, Han S, Carass A, et al. Brain ventricle parcellation using a deep neural network: Application to patients with ventriculomegaly. Neuroimage Clin 2019;23:101871.
31. Zhou X, Ye Q, Jiang Y, et al. Systematic and comprehensive automated ventricle segmentation on ventricle images of the elderly patients: a retrospective study. Front Aging Neurosci 2020;12:618538.
32. Sander L, Pezold S, Andermatt S, et al. Accurate, rapid and reliable, fully automated MRI brainstem segmentation for application in multiple sclerosis and neurodegenerative diseases. Hum Brain Mapp 2019;40(14):4091–4104.
33. Magnusson M, Love A, Ellingsen LM. Automated brainstem parcellation using multi-atlas segmentation and deep neural network. In: Landman BA, Išgum I, eds. Medical Imaging 2021: Image Processing. Online Only, United States: SPIE, 2021; 82.
34. Despotović I, Goossens B, Philips W. MRI segmentation of the human brain: challenges, methods, and applications. Comput Math Methods Med 2015;2015:450341.
35. Fischl B. FreeSurfer. Neuroimage 2012;62(2):774–781.